Hydrodechlorination of carbon tetrachloride with nanoscale nickeled zero-valent iron @ reduced graphene oxide: kinetics, pathway, and mechanisms

Xiao Chen, Zhen Wang, Qi Yang, Yeyao Wang, Zhaoxiang Liu and Zhilin Yang

ABSTRACT

In recent years, carbon tetrachloride (CT) has been frequently detected in surface water and groundwater around the world; it is necessary to find an effective way to treat wastewater contaminated with it. In this study, Ni/Fe bimetallic nanoparticles were immobilized on reduced graphene oxide (NF@rGO), and used to dechlorinate CT in aqueous solution. Scanning electron microscopy (SEM) demonstrated that the two-dimensional structure of rGO could disperse nanoparticles commendably. The results of batch experiments showed that the $4N_4F$@rGO (Fe/GO = 4 wt./wt., and Ni/Fe = 4 wt.%) could reach a higher reduction capacity (143.2 $mg_{CT}/g_{catalyst}$) compared with Ni/Fe bimetallic nanoparticles (91.7 $mg_{CT}/g_{catalyst}$) and Fe^0 nanoparticles (49.8 $mg_{CT}/g_{catalyst}$) respectively. That benefited from the nickel metal as a co-catalyst, which could reduce the reaction activation energy of 6.59 kJ/mol, and rGO as an electrical conductivity supporting material could further reduce the reaction activation energy of 4.73 kJ/mol as presented in the conceptual model. More complete dechlorination products were generated with the use of $4N_4F$@rGO. Based on the above results, the reductive pathway of CT and the catalytic reaction mechanism have been discussed.

Key words | carbon tetrachloride, degradation kinetics, nanoparticles, Ni/Fe bimetal, reduced graphene oxide

Xiao Chen
Zhen Wang
Qi Yang (corresponding author)
Zhilin Yang
Beijing Key Laboratory of Water Resources & Environmental Engineering,
China University of Geosciences (Beijing),
Beijing 100083,
China
E-mail: *yq@cugb.edu.cn*

Yeyao Wang
China National Environmental Monitoring Center,
Beijing, 100012,
China

Zhaoxiang Liu
Foreign Economic Cooperation Office,
Ministry of Environmental Protection,
Beijing, 100035,
China

HIGHLIGHTS

- Ni/Fe nanoparticles were evenly immobilized on reduced graphene oxide (NF@rGO).
- NF@rGO dramatically accelerated the hydrogenolysis pathway of carbon tetrachloride.
- More hazardous intermediate products were reduced with the presence of NF@rGO.
- Atomic hydrogen as a powerful reducing agent was involved in the dechlorination process.
- The catalytic activities of two catalysts with different supporters were compared.

doi: 10.2166/wst.2020.386

GRAPHICAL ABSTRACT

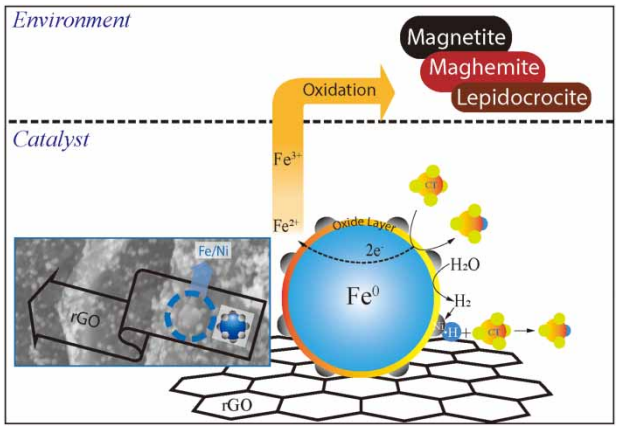

INTRODUCTION

Carbon tetrachloride (CT) was widely used in the past as a cleaning and degreasing solvent in industry due to its ability to dissolve a wide range of organic substances. The widespread use of CT led to its dispersion in the environment persistently (Doherty 2000). Due to the adverse health effects of CT on humans and animals, such as central nervous system depression, liver and kidney damage, CT has been established as a class of priority pollutants prohibited by the US EPA (Hua & Hoffmann 1996). However, chloroform (CF) as a reduction product of CT is more toxic (Semprini & McCarty 1992). Therefore, it is of great significance to develop an efficient method for transforming CT into non-hazardous products.

In general, degradation of CT via biological methods always requires quite a long time (Hashsham *et al.* 1995), and may have the risk of poisoning the organism in some situations (Santharam *et al.* 2014), which strongly restricts its application field. Boronina & Klabunde (1995) found that three zero-valent metals (magnesium, tin and zinc) can be used to reduce CT in aqueous solutions. Feng & Lim (2005) found that although Zn could reduce CT with a high reaction rate compared with Fe powder, it was hard to reduce CT to complete dechlorination products (CDCPs) during the reaction. Due to the low-cost and high efficiency, zero-valent iron (ZVI) has been widely investigated in the wastewater treatment of chlorinated organic compounds (COCs) (Gillham & Ohannesin 1994; Matheson & Tratnyek 1994; Balko & Tratnyek 1998; Cwiertny *et al.* 2006). Among these, nanoscale zero-valent iron (nZVI) has particularly attracted considerable attention due to its large specific surface area (Zhang 2003). However, this advantage could not be fully exploited while in practice (Liu & Lal 2012), such as nZVI easily formed a magnetic passive layer which blocked the reactive sites and resulted in aggregation of the nanoparticles (NPs) (Zhang *et al.* 2002). Therefore, it is highly required to develop a new composite catalyst to improve the catalytic activity of nZVI.

Recently, various support materials have been developed to prevent particle aggregation (e.g. MWCNTs, activated carbon, SiO_2, carboxymethylcellulose, Fe_3O_4) (Kustov *et al.* 2014; Jin *et al.* 2018; Lv *et al.* 2018; Wu *et al.* 2018; Chen *et al.* 2019). Beyond these, graphene as a supporting material holds excellent mechanical, electrical and thermal characteristics, which is superior to other traditional materials (Dreyer *et al.* 2009). In order to obtain a similar structure to pristine graphene, reduced graphene oxide (rGO) was synthesized from graphite flake via a chemical method. It has some excellent characteristics: (1) the high specific surface area of the two-dimensional structure could allow nanoparticle catalyst to be efficiently loaded on it (Bai & Shen 2012), (2) the conjugated structure of graphene could enhance the adsorption capacity of the reactant molecules (Zhang *et al.* 2012), (3) the oxygen-containing groups could make the layers hydrophilic (Pei & Cheng 2012), (4) the characteristics of electrical conductivity were favorable during the catalytic reaction (Stankovich *et al.* 2007).

Deposition of a second metal (e.g. Ni, Pd, Cu, Co, Au and Pt) as a co-catalyst onto the surface of iron is a general process to enhance the dechlorination efficiency and

reaction rate (Cwiertny *et al.* 2006). Therein, Pd/Fe bimetal greatly improved the dechlorination efficiency of COCs; however, nickel as a non-precious metal could replace palladium metal without loss of performance (Zhang *et al.* 1998). As a result of lower hydrogen overpotential, Ni as a co-catalyst accelerated the hydrogen production process compared with single Fe, and the produced H_2 could reduce COCs indirectly with the existence of an effective catalyst (e.g. Pd, Ni, Cu and Co) (Matheson & Tratnyek 1994; Schreier & Reinhard 1995; Lowry & Reinhard 1999; Schrick *et al.* 2002). For this reason, we chose Ni as a cost-effective metal dopant on nZVI particles to improve the reactivity of the catalyst.

In this study, nanoscale nickeled zero-valent iron @ rGO (NF@rGO) composite was synthesized, characterized and used to degrade CT. Batch experiments evaluated the removal capacity and the catalytic activity of laboratory-synthesized catalysts; besides that, the reduction products of CT and its reaction kinetics were studied. Catalyst characterization was carried out by X-ray diffraction (XRD), X-ray photo-electron spectroscopy (XPS) and scanning electron microscope (SEM) with X-ray energy dispersive spectroscopy (EDS). The purpose of our work was to develop a highly active catalyst, and provide a theoretical reference for the catalytic hydrodechlorination of COCs.

EXPERIMENT

Material and chemicals

All the chemicals used were of analytical reagent (AR) grade from commercial sources. Graphite flake (purity $\geq$ 99.8%, −325 mesh), $NaNO_3$ (≥99.5%), H_2SO_4 (5 and 98%), $KMnO_4$ (≥98.0%), H_2O_2 (30%) and HCl (5%) were used to synthesize graphene oxide. $FeSO_4{\cdot}7H_2O$ (≥99.5%). $NiSO_4{\cdot}6H_2O$ (≥98.5%) and $NaBH_4$ (≥ 99.5%) were used to synthesize NF@rGO. All degradation experiments used a certain volume of freshly made stock solution of CT (15 mg/L). All deionized (DI) water was prepared with an Aquelix 5 (Millipore) pure water system and bubbled with nitrogen (99.2%) before use.

Synthesis of GO

The graphene oxide (GO) was prepared by Hummers method, and the whole process was carried out in an Erlenmeyer flask with water bath and magnetic stirring. Firstly, graphite flake (1 g) and $NaNO_3$ (0.5 g) powder were mixed by using H_2SO_4 aqueous solution (23 mL, 98%). After 1 h stirring at 0 °C, 3 g of $KMnO_4$ was divided into 6 parts and add to the dispersion within 2.5 h at 10–15 °C. Subsequently, the temperature of the water bath was adjusted to 35 °C and it was stirred for 24 h, and then the temperature was increased to 90 °C. Meanwhile, H_2SO_4 aqueous solution (100 mL, 5%) and deionized water (150 mL) was added to the mixture respectively for further dilution of the dispersion. After the H_2O_2 aqueous solution (5 mL, 30%) was added to the suspension, the resultant GO was immediately filtrated (using 20 μm qualitative filter paper) until the suspension stopped bubbling, and it was washed with HCl aqueous solution (5%) and DI water (until no SO_4^{2-} was detected in the supernate fluid). Finally, the dried GO powder was obtained with a vacuum oven (60 °C for 48 h).

Synthesis of NF@rGO

The NF@rGO was synthesized in a nitrogen atmosphere through a two-step reductive deposition method, and the whole process was carried out in a four-necked flask with continuous stirring; various composition ratios (Fe/GO = 2:1, 3:1, 4:1 and 5:1 wt./wt.) were considered. First of all, GO was added to DI water to form a suspension buffer (0.75 g/L) with ultrasonic dispersion, and 100 mL of corresponding mass of $FeSO_4{\cdot}7H_2O$ aqueous solution was added dropwise into the solution with a peristaltic pump at the speed of 20 rpm. And then, $NaBH_4$ aqueous solution (10.0 g/L) was added dropwise into the solution. At the end of dripping, ferrous iron and GO were reduced by $NaBH_4$ and then nZVI particles were co-precipitated with rGO. The mechanism is $NaBH_4$, as a strong reducing reagent, could be effective in reducing the carbonyl group to the alcohol group of GO (Periasamy & Thirumalaikumar 2000), and the reaction equation of ferrous iron reduced by $NaBH_4$ is described as follows:

$$Fe(H_2O)_6^{2+} + 2BH_4^- \rightarrow Fe^0 \downarrow + 2B(OH)_3 + 7H_2 \uparrow \quad (1)$$

Secondly, the nZVI@rGO was collected by magnetic separation and washed with absolute ethyl alcohol repeatedly. After that, the semi-finished product was put into a four-necked flask using DI water. And then the $NiSO_4{\cdot}6H_2O$ aqueous solution was dropwise added into the solution to coat a thin layer of nickel on the surface of the nZVI particles. The method is according to the following equations for chemical reactions:

$$Ni^{2+} + Fe^0 \rightarrow Ni \downarrow + Fe^{2+} \quad (2)$$

At last, the NF@rGO NPs were washed and freeze-dried for further use. Similarly, nZVI and Ni/Fe bimetallic NPs were also prepared with this procedure. The preparation method of $2N_4F$@MWCNTs (Fe/MWCNTs = 2 wt./wt., Ni/Fe = 4 wt.%) was according to our previous work (Chen *et al.* 2019).

Catalyst characterization

The surface morphology of nZVI, GO and NF@rGO was characterized by scanning electron microscope (SEM) (Hitachi, SU-8010, Japan), the Ni content of Ni/Fe bimetal was quantified by X-ray energy dispersive spectroscopy (EDS) (Horiba, Japan). The mineralogical properties of nZVI, fresh and used NF@rGO, were investigated by X-ray diffraction (XRD) (Bruker, AXS, D8 Advance). The chemical states of NF@rGO were examined by X-ray photo-electron spectroscopy (XPS) (Thermo Scientific, ESCALAB 250 XI).

Experimental system

A series of batch experiments were conducted to study the catalytic activity of laboratory-synthesized catalysts and investigate the intermediate products of CT degradation. All of the experiments were carried out in 100 mL serum bottles with a rotary shaker (220 rpm), each bottle was double sealed, Teflon-lined and had an aluminum cap, and each experiment was run in triplicate. Before the experiment, 0.01 g of laboratory-synthesized catalysts were added in the serum bottle respectively with 15 mg/L of CT stock solution until no headspace was left. At specific time intervals, 1 mL of samples were filtered with 0.22 μm filters and withdrawn to bottle headspace for analysis the concentration of CT and its degradation products by gas chromatography spectrometry (GC-2014, Shimadzu, Japan). In addition, the generated CH_4 and CO in the bottle were gathered with an aluminum foil gas-collecting bag.

The sample from bottle headspace was determined by GC with electron capture detector (ECD). Samples were separated and evaluated with a Rtx-1 column (30.0 m × 0.25 mm ID × 0.25 μm thickness, Restek, USA), with nitrogen (99.99%) as the carrier gas. The oven temperature was programmed from 40 to 100 and finally to 200 °C at the rate of 8 and 6 °C/min, with a 5 min initial hold and 10 min final hold. The temperature of injector and detector were 220 and 320 °C, respectively.

Besides, the sample from the gas-collecting bag was determined by GC with a thermal conductivity detector (TCD). Samples were separated and evaluated with a TDX-01 column (2.0 m × 3.00 mm, China), with helium (99.99%) as the carrier gas. The oven temperature was 120 °C, held for 7 min, and the temperatures of the injector and detector were 100 and 150 °C, respectively. Blank experiments and repeated experiments were carried out and the results are described in the Supplementary Information.

RESULTS AND DISCUSSION

Characterization of catalysts

XRD measurement

The XRD patterns in Figure 1 were determined to identify the crystal structures of nZVI, fresh and used $4N_4F$@rGO (Fe/GO = 4:1 wt./wt., Ni/Fe = 4 wt.%). The sharp and strong diffraction peaks at $2\theta = 44.62°$ and 65.03° corresponded to the standard card of α-Fe (JCPDS, No. 06-0696). However, the intensity of the reflection peak at $2\theta = 44.62°$ decreased significantly in fresh $4N_4F$@rGO, this may be caused by the small crystallites of Fe^0 particles.

Besides, it was noteworthy that the reflection peaks at $2\theta = 27.55°$, 36.29° and 46.91°, which belonged to aged $4N_4F$@rGO, corresponded to the standard card of lepidocrocite (γ-FeOOH) (JCPDS, No. 44-1415) and were assigned to the (210), (301) and (020) planes, respectively. The reflection peaks at $2\theta = 30.07°$, 35.87°, 56.91°, 62.50° corresponding to magnetite (Fe_3O_4) (JCPDS, No. 19-0629) were assigned to the (220), (311), (511) and (440) planes, and/or maghemite (γ-Fe_2O_3) (JCPDS, No. 25-1402), assigned to the (206) and (119) planes. The results exposited that the Fe^0 was oxidized and deposited on the surface of $4N_4F$@rGO in the process of reaction.

However, no obvious characteristic diffraction peaks of Ni or graphite were detected either in fresh or recycled $4N_4F$@rGO, which was due to the diffraction peaks of nickel metal being very close to iron, and graphene sheets were prevented from forming a regular crystal structure as a result of the inserted NPs.

XPS characterization

In order to get more information on the chemical composition of NF@rGO, XPS analyses were performed to evaluate the chemical states including Ni, Fe, O and C (Figure 2(a)).

According to Ni 2p spectrum (Figure 3(b)), the photoelectron peaks located at 852.4 and 869.0 eV demonstrated the existence of Ni ($Ni2p_{3/2}$, 852.3 eV; $Ni2p_{1/2}$, 869.7 eV)

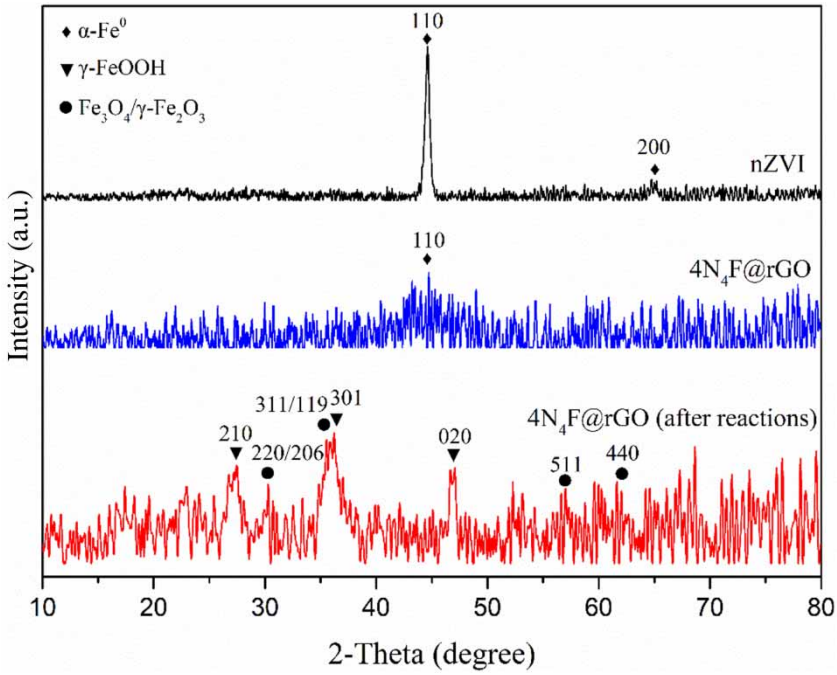

Figure 1 | XRD patterns for nZVI, fresh and aged $4N_4F$@rGO.

(Moulder *et al.* 1979), and the peaks of NiO ($Ni2p_{3/2}$, 853.3 eV; $Ni2p_{1/2}$, 871.7 eV) (Moulder *et al.* 1979) were also detected at 854.2 and 870.6 eV.

Meanwhile, Figure 2(c) shows the high-resolution spectrum of Fe2p, two photoelectron peaks at 710.5 and 723.9 eV demonstrate the existence of oxidized iron (Fe(III) and Fe(II)), which are similar to magnetite (Fe_3O_4) ($Fe2p_{3/2}$, 710.6 eV; $Fe2p_{1/2}$, 724.1 eV) (Fiedor *et al.* 1998), hydrated ferric oxide (FeOOH) ($Fe2p_{3/2}$, 711.2 eV; $Fe2p_{1/2}$, 724.9 eV) (Echigo *et al.* 2012), hematite (α-Fe_2O_3) ($Fe2p_{3/2}$, 711.0 eV; $Fe2p_{1/2}$, 724.6 eV) (Yamashita & Hayes 2008) and maghemite (γ-Fe_2O_3) ($Fe2p_{1/2}$, 710.9 eV) (Zhang *et al.* 2011). Moreover, Fe^0 showed an obvious peak at 706.7 eV followed by its satellite peak at 719.5 eV ($Fe2p_{3/2}$, 706.75; $Fe2p_{1/2}$, 719.95 eV) (Moulder *et al.* 1979).

The O (1 s) spectrum (Figure 2(d)) showed three types of oxygen species, which corresponded to the anionic oxygen in Fe_XO_Y (530.7 eV), the oxygen-containing functional groups in rGO (531.9 eV) (Fan *et al.* 2011), and the adsorbed H_2O (536.0 eV) (Ertl *et al.* 1997).

The C (1 s) spectra (Figure 2(e)) presented four types of carbon bonds (Moulder *et al.* 1979; Ertl *et al.* 1997; Hayes 2001): (1) non-oxygenated carbon (including C-C, C = C, and C-H) (284.4 eV), (2) the carbon in C-O (C-O-C and/or C-OH groups) (285.4 eV), (3) the carbonyl carbon in C = O (287.8 eV), (4) carboxylate carbon in O-C = O (288.9 eV). The peak area of C-C was greater than other carbon-based oxygen-containing functional groups, which proved that GO was successfully reduced to rGO by $NaBH_4$ during the preparation of the catalyst.

SEM characterization

The SEM image of nZVI (a), rGO (b), $4N_4F$@rGO (c, d) is presented in Figure 3; the partition ratio of the alloy element (corresponding to the box in part d) was measured and is presented in Figure 3(e). It can be seen that nZVI particles interconnected to form a necklace-like structure due to surface tension and magnetic interactions between each particle. Figure 3(b) exhibits the sheet-like structures of GO. Moreover, it can be clearly seen $4N_4F$@rGO from Figure 3(c) and 3(d) that the Ni/Fe bimetal particles were evenly distributed on the surface of rGO. The EDS analysis indicated that the NPs were Ni/Fe bimetal and reached a desirable ratio.

Batch experiments

Loading ratio of rGO

Various mass of Ni/Fe bimetallic NPs (Ni/Fe = 4 wt.%) were loaded onto the surface of rGO. As shown in Figure 4, the reduction of CT followed pseudo-first-order kinetics,

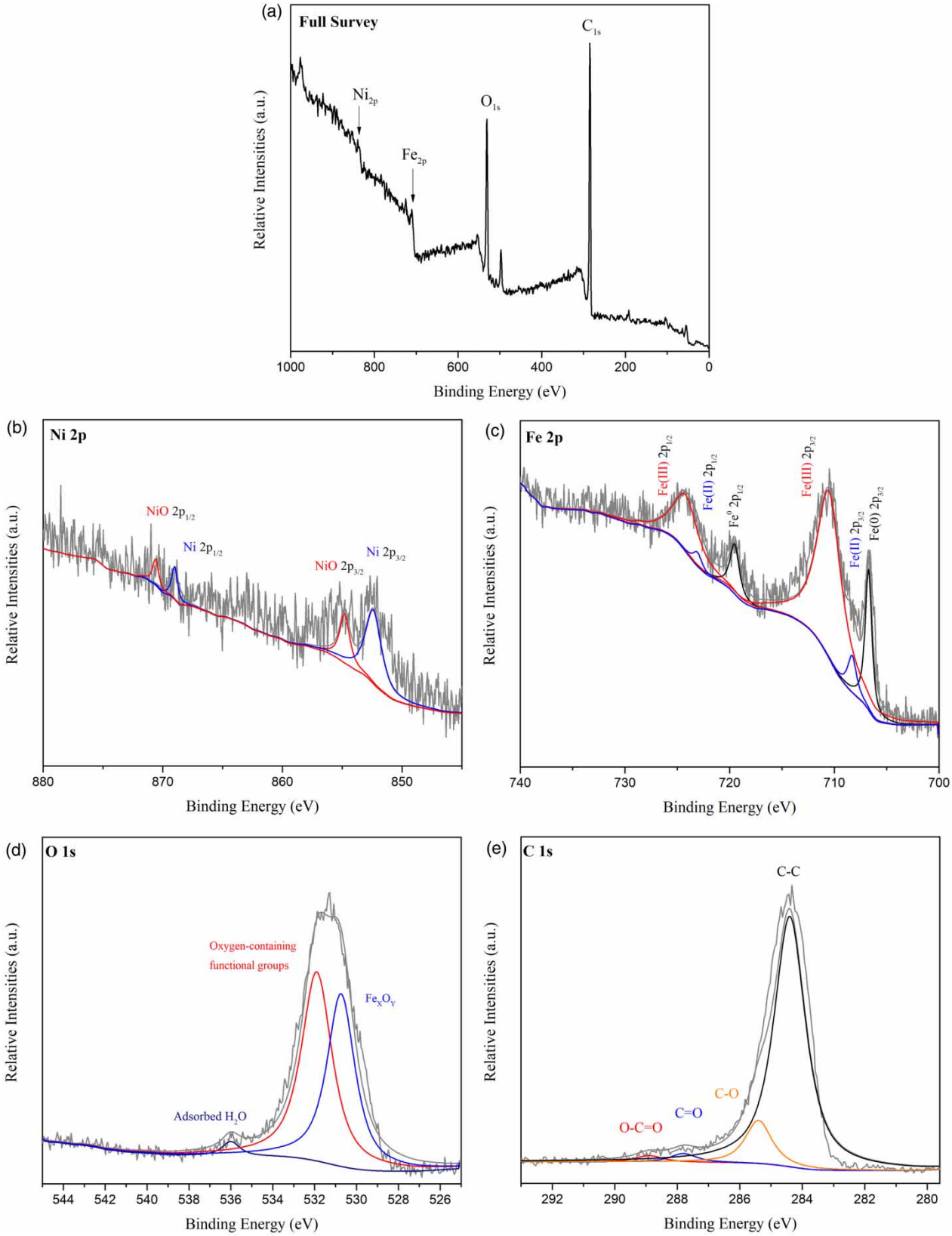

Figure 2 | (a) Full survey XPS patterns for $4N_4F$@rGO, (b)–(e) high-resolution XPS patterns for $4N_4F$@rGO of Ni (2p), Fe (2p), O (1 s) and C (1 s).

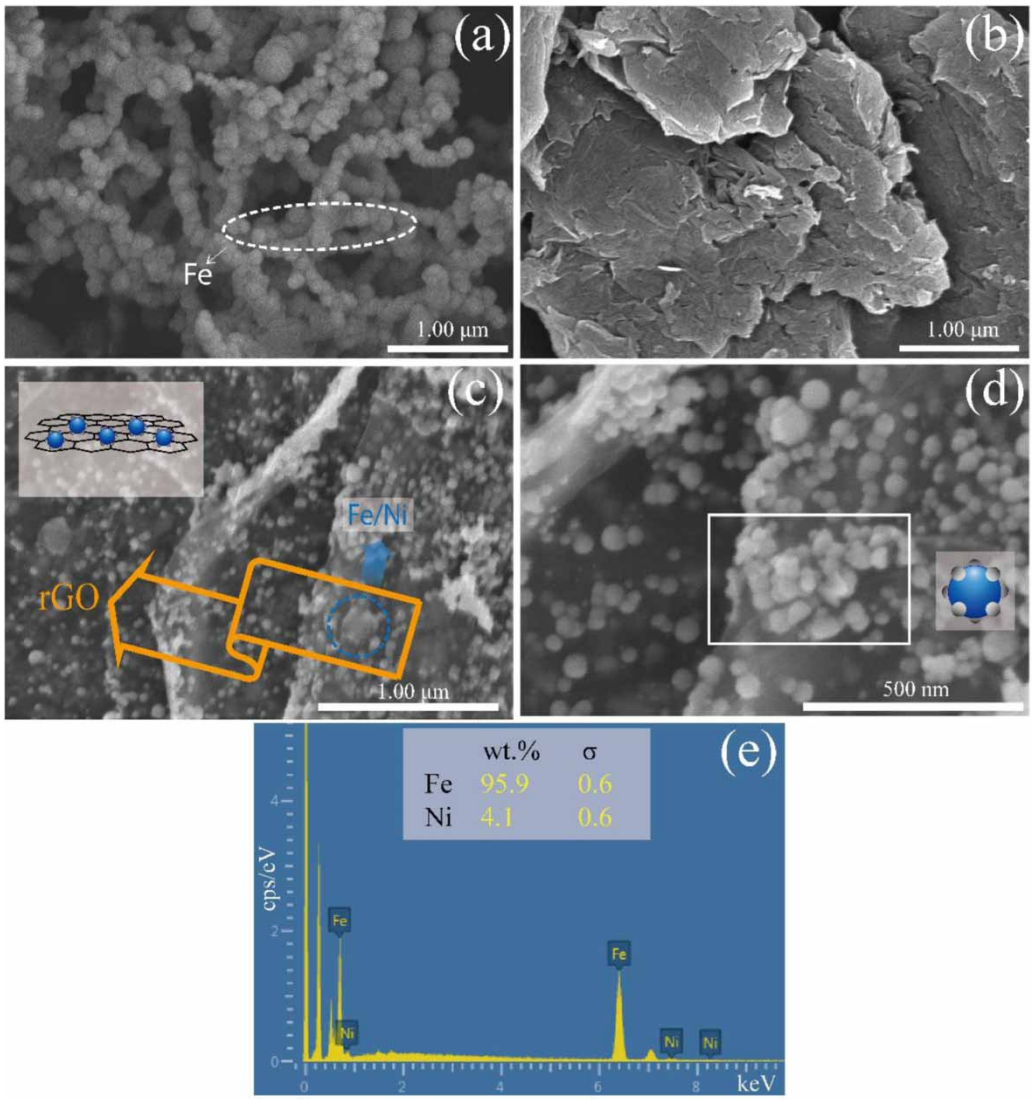

Figure 3 | (a) SEM images of nZVI, (b) rGO, (c, d) $4N_4F$@rGO and (e) EDS spectra of the metal composition of $4N_4F$@rGO (corresponding to the box in part d).

$4N_4F$@rGO (Fe/GO = 4 wt./wt., Ni/Fe = 4 wt.%) reached a higher efficiency in CT degradation.

Furthermore, the properties of four laboratory-synthesized catalysts were investigated by calculating the removal capability (mg $_{CT}$/g $_{catalyst}$). The results of the calculation are listed in Table 1; $4N_4F$@rGO could degrade CT with a high removal rate in 35 min, the observed rate constant (k_{obs}) indicated that the reaction rate of $4N_4F$@rGO was 10 times that of nZVI. By comparison with the removal capability and reaction rate, $4N_4F$@rGO achieved better results than $2N_4F$@MWCNTs (Fe/MWCNTs = 2 wt./wt., Ni/Fe = 4 wt.%) in CT degrading, which means rGO as a supporter could be loaded with more metal to improve its catalytic performance.

Reaction activation energy

The degradation of CT by nZVI, N_4F and $4N_4F$@rGO was fitted to the pseudo first-order kinetic model, the experimental results are summarized in Table 2 and Figure S3 (in the Supplementary Information). The kinetic model was used to simulate the relationships between the reaction rate and temperature (Figure 5) for obtaining the activation energy via the Arrhenius equation (Dahm 1994):

$$K = A \times e^{-\frac{E_a}{RT}} \quad (3)$$

where K stands for the pseudo-first-order rate constant, A for the frequency factor, R for the universal gas constant

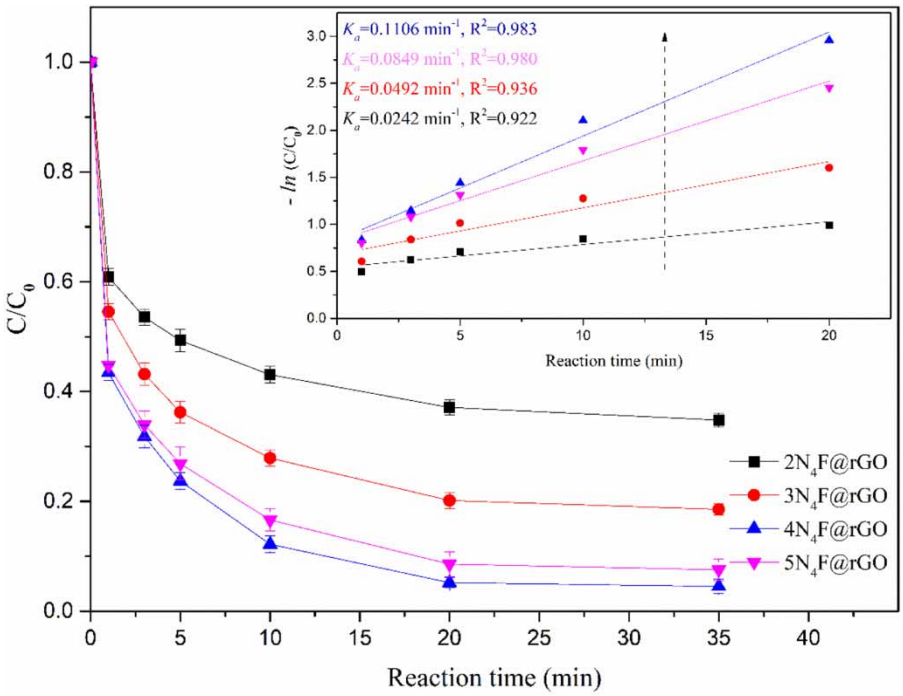

Figure 4 | Different loading ratio of Ni/Fe bimetal on rGO.

(8.314 J·mol^{-1} K^{-1}), T for the temperature (K), and then the value of activation energy (E_a) can be obtained by calculating the slope of the plot line via the following equation:

$$\ln K = -\frac{E_a}{R} \times \frac{1}{T} + \ln\ A \tag{4}$$

Figure 5(d) clearly demonstrates that nickel as a co-catalyst decreased the activation energy of 6.59 kJ/mol in N_4F compared with nZVI, and rGO as a conductive material could further reduce the activation energy of 4.73 kJ/mol by accelerating electron transfer during the redox reaction.

Reduction products and pathway of CT

In order to explore the reduction pathway of CT, various products were monitored by GC in the process of reaction, including chloroform (CF), dichloromethane (DCM), carbon monoxide (CO) and methane (CH_4), trace amounts (around the detection limit of GC) of perchloroethylene (PCE) and trichloroethylene (TCE) were also detected after a certain time of reaction. Among these, CO and CH_4 may be considered as complete dechlorination products (CDCPs).

As shown in Figure 6, for CF as a daughter product from CT, the amount decreased significantly after 10 min in $2N_4F$@MWCNTs and $4N_4F$@rGO catalytic system; however, DCM was hardly further reduced by these two catalysts within 2 h through independent experiments, so the generated CDCPs were attributed to the reduction products of CF. It is noteworthy that CDCPs were not detected in the nZVI catalytic system during the experimental period, which means Ni as a co-catalyst could promote the generation of CDCPs. Besides, benefiting from the high reactivity of $2N_4F$@MWCNTs and $4N_4F$@rGO, considerable amounts of CDCPs were produced in 2 h.

Based on the kinds of degradation products and the concentration variation, it was inferred that the reduction pathway of CT was initiated by dissociative electron transfer based on carbon-centered radical (Balko & Tratnyek 1998):

$$CCl_4\ (\text{or}\ \ CHCl_3) + e^- \rightarrow \cdot CCl_3\ (\text{or} \cdot CHCl_2) + Cl^- \tag{5}$$

Table 1 | Results of laboratory-synthesized catalysts on degradation of CT[a]

Catalyst	Removal rate (%)	Removal capability (mg/g)	k_{obs} (min^{-1})
nZVI	37.2	55.8	0.0102
N_4F	61.2	91.7	0.0267
$2N_4F$@MWCNTs	90.8	136.2	0.1073
$4N_4F$@rGO	95.5	143.2	0.1106

[a]Reaction conditions: initial concentration of CT = 15 mg/L, catalyst dosage = 0.1 g/L, initial pH = 7.0, reaction time = 35 min and the temperature was 30 °C.

Table 2 | Results of laboratory-synthesized catalysts on degradation of CT under different temperature[b]

	nZVI		N_4F		$4N_4F$@rGO	
T (K)	Removal rate (%)	K_a (min^{-1})	Removal rate (%)	K_a (min^{-1})	Removal rate (%)	K_a (min^{-1})
283.15	21.7	0.0030	27.7	0.0082	69.8	0.0340
293.15	29.1	0.0053	41.8	0.0140	83.3	0.0607
303.15	37.2	0.0102	61.2	0.0267	95.5	0.0926
308.15	46.2	0.0163	68.9	0.0345	98.3	0.1268
313.15	54.0	0.0219	81.0	0.0452	99.0	0.1616

[b]Reaction conditions: initial concentration of CT = 15 mg/L, catalyst dosage = 0.1 g/L, initial pH = 7.0 and reaction time = 35 min.

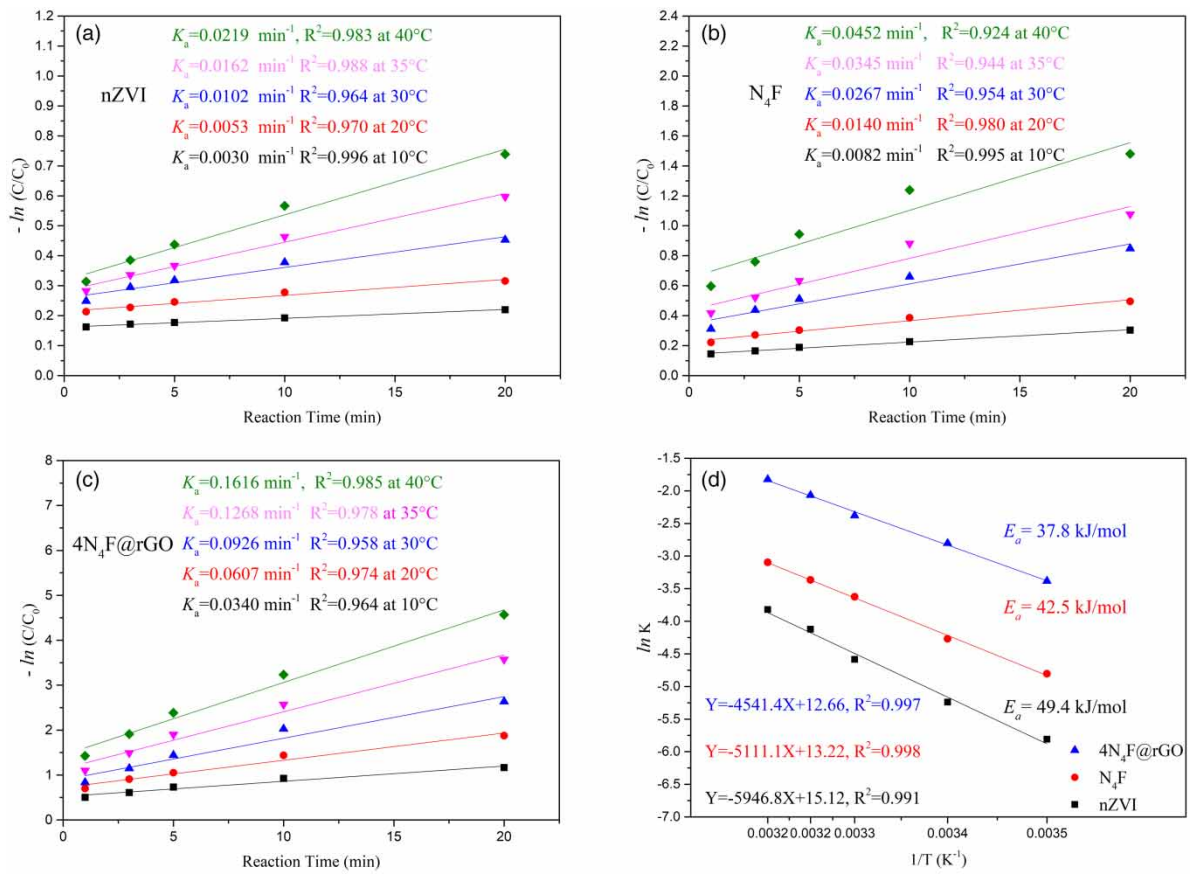

Figure 5 | Kinetic analysis of (a) nZVI, (b) N4F, (c) 4N4F@rGO under different temperatures, and fitting curve of ln(K)/T (d).

The resulting trichloromethyl radicals (or dichloromethyl radicals) can be further electronically transferred to produce CF (or DCM):

$$\cdot CCl_3 \text{ (or } \cdot CHCl_2) + e^- + H^+ \rightarrow CHCl_3 \text{ (or } CH_2Cl_2) \quad (6)$$

It was inferred that the generated CDCPs were the reduction products of CF, CF was degraded by losing a proton first and then a chloride ion to form dichlorocarbene (Satterfield 1991):

$$CHCl_3 \rightarrow (:CCl_3)^- + H^+ \rightarrow :CCl_2 + Cl^- + H^+ \quad (7)$$

The dichlorocarbene was then hydrolyzed to form CO, and CO could be further reduced to methane via

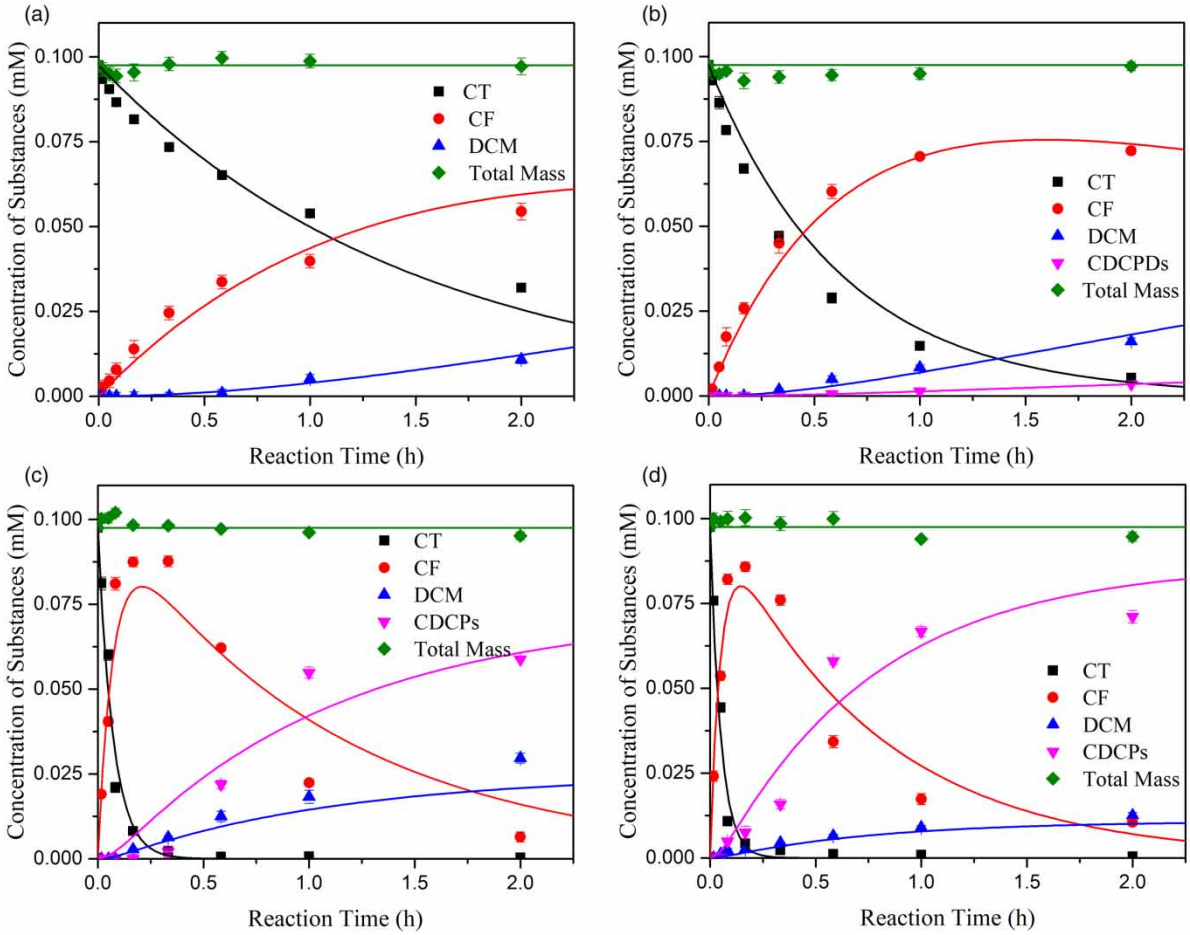

Figure 6 | The changes of substrate concentration in various catalytic reduction systems: (a) nZVI, (b) N4F, (c) $2N_4F$@MWCNTs and (d) $4N_4F$@rGO.

Fischer–Tropsch process (Smith & March 2001):

$$:CCl_2 + H_2O \rightarrow CO + 2Cl^- + 2H^+ \quad (8)$$

$$3H_2 + CO \xrightarrow{\text{catalyst}} CH_4 + H_2O \quad (9)$$

The detected perchloroethylene (PCE) may be formed by dimerization of dichlorocarbene radicals, and trichloroethylene (TCE) should be the reduction product of PCE.

$$2\ :CCl_2 \rightarrow C_2Cl_4 \quad (10)$$

Kinetics of CT reduction

According to the reaction equations (Equations (5)–(9)), the major reduction pathway of CT could be described by Figure 7. Based on the pseudo first-order kinetic model, the rate equations of CT reduction can be expressed as follows:

$$\frac{dC_{CT}}{dt} = -k_1 C_{CT} \quad (11)$$

$$\frac{dC_{CF}}{dt} = k_1 C_{CT} - k_2 C_{CF} - k_3 C_{CF} \quad (12)$$

$$\frac{dC_{DCM}}{dt} = k_2 C_{CF} \quad (13)$$

$$\frac{dC_{CDCPs}}{dt} = k_3 C_{CF} \quad (14)$$

where C is the concentration of CT and its reduction products, the values of k_1-k_3 can be obtained by fitting the

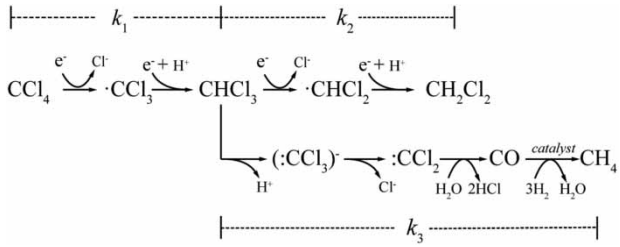

Figure 7 | Reduction process of CT.

Table 3 | Simulated rate constants of CT reduction processes with various catalysts

Catalysts	k_1 (h^{-1})	k_2 (h^{-1})	k_3 (h^{-1})
nZVI	0.57	0.16	0.00
N_4F	1.60	0.15	0.01
$2N_4F$@MWCNTs	13.87	0.24	0.70
$4N_4F$@rGO	19.81	0.15	1.20

experimental data with the curve of the following equation:

$$C_{CT} = C_{CT_0} e^{-k_1 t} \quad (15)$$

$$C_{CF} = \frac{k_1}{k_2 + k_3 - k_1} \left[e^{-k_1 t} - e^{-(k_2+k_3)t}\right] C_{CT_0} \quad (16)$$

$$C_{DCM} = \frac{k_1 k_2}{k_2 + k_3 - k_1} \left[\frac{-1}{k_1} e^{-k_1 t} + \frac{1}{k_2 + k_3} e^{-(k_2+k_3)t} + \frac{1}{k_1} - \frac{1}{k_2 + k_3}\right] C_{CT_0} \quad (17)$$

$$C_{CDCPs} = \frac{k_1 k_3}{k_2 + k_3 - k_1} \left[\frac{-1}{k_1} e^{-k_1 t} + \frac{1}{k_2 + k_3} e^{-(k_2+k_3)t} + \frac{1}{k_1} - \frac{1}{k_2 + k_3}\right] C_{CT_0} \quad (18)$$

The fitting curve of the rate equations is shown in Figure 6. The variance was used as a criterion to select the best set of rate constants (all of the R^2 were greater than 0.92), and the k values are listed in Table 3.

Table 3 reveals that all CT were reduced through the hydrogenolysis pathway to CF and DCM by these four catalysts. However, the presence of nickel not only accelerated the reduction of CT to CF, but also promoted the complete reduction pathway of CF. Moreover, N_4F obtained more reactive sites due to immobilization on rGO, greatly increasing the reaction rate of CT reduction, including reduction of CT to CF (k_1) and reduction of CF ($k_2 + k_3$). As a result, rGO could support more N_4F NPs, $4N_4F$@rGO has the capability of reducing more CF to CDCPs (k_3).

Mechanism of CT reduction by $4N_4F$@rGO

As shown in Figure 8, the reduction of CT by $4N_4F$@rGO in aqueous solution involved four reactions. In the Fe-H_2O system, Fe^0 serving as electron donor could directly react with COCs:

$$Fe^0 + RCl + H^+ \rightarrow Fe^{2+} + RH + Cl^- \quad (19)$$

Meanwhile, Fe^{2+} as the oxidation product of Fe^0 could still be involved in the reduction of COCs (Equation (20)). However, this reaction occurred slowly due to the lower electron-donating ability of Fe^{2+} (E_0 (Fe^{2+}/Fe^0) = −0.440 V, E_0 (Fe^{3+}/Fe^{2+}) = +0.770 V). This process can be demonstrated by the formation of a passivation layer, which contained trivalent iron on the surface of the $4N_4F$@rGO after repeated use.

$$2Fe^{2+} + RCl + H^+ \rightarrow 2Fe^{3+} + RH + Cl^- \quad (20)$$

A benefit from nickel metal is that it has lower hydrogen overpotential compared with iron. Ni/Fe bimetal could accelerate the indirect reduction of COCs by the hydrogen produced (Equation (21)). Nickel metal is indispensable in the process of hydrogen reduction, H_2 could not reduce COCs directly in the absence of an effective catalyst (e.g. Pd, Ni, Cu and Co). The generated hydrogen could be embedded in the crystal lattice of Ni to form reactive

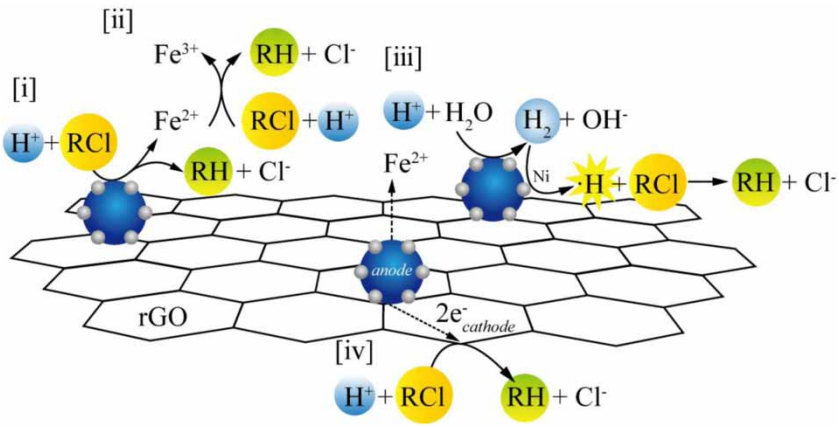

Figure 8 | Mechanism of CT reduction by $4N_4F$@rGO.

atomic hydrogen (·H) (Equations (23)–(25)) (Cwiertny *et al.* 2006), and ·H as a very powerful reducing agent played an important role in the complete dechlorination of CT (Wang *et al.* 2009).

$$Fe^0 + H_2O + H^+ \rightarrow Fe^{2+} + H_2 + OH^- \quad (21)$$

$$Ni + H_2 \rightarrow Ni \cdot H_2 \quad (22)$$

$$Ni + RCl \rightarrow Ni \cdots Cl \cdots R \quad (23)$$

$$Ni \cdot H_2 + Ni \cdots Cl \cdots R \rightarrow RH + H^+ + Cl^- + 2Ni \quad (24)$$

$$\cdot H + RCl + e^- \rightarrow RH + Cl^- \quad (25)$$

As a carbon material, rGO can form primary batteries with Fe^0 in aqueous solution. In the process of redox reaction, the electrons transferred from anode (Fe^0) to cathode (rGO), COCs as the electron acceptor could be reduced at the surface of rGO without contact with Fe^0:

$$Fe^0 - 2e^- \rightarrow Fe^{2+} \quad (26)$$

$$RCl + 2e^- + H^+ \rightarrow RH + Cl^- \quad (27)$$

CONCLUSION

In this research, $4N_4F$@rGO has been successfully synthesized by a two-step method and its removal capacity and CT reduction rate was assessed and compared with three other laboratory-synthesized catalysts. The results suggested that $4N_4F$@rGO can degrade CT with a high reaction rate and selectivity towards non-chlorinated products. Furthermore, nickel metal reduced the active energy and accelerated the complete dechlorination reaction by the H-radical produced, and the Ni/Fe bimetal gained more reactive sites by loading on rGO to further accelerate the reduction of CT to CDCPs.

Based on the kinds of degradation products of CT and its concentration variation in reduction experiments, it was inferred that the reduction process of CT was initiated by dissociative electron transfer based on carbon-centered radicals. Meanwhile, the mechanism of CT reduction by $4N_4F$@rGO was also discussed, it was concluded that rGO as an excellent electroconductive supporter could not only disperse the bimetal but also participated in the galvanic interaction with Fe^0 to reduce CT indirectly.

The catalytic activities of two catalysts ($4N_4F$@rGO and $2N_4F$@MWCNTs) with different supporters were compared. It was found that rGO could load more Ni/Fe and provide a better fluidity for substrate, which was conducive to reduce more intermediate products to CDCPs.

ACKNOWLEDGEMENTS

This work was supported by the National Natural Science Foundation of China (50578151), the National Science and Technology Major Project of China (2009ZX07207-008, 2009ZX07419-002, 2009ZX07207-001), the Beijing Municipal Education Commission School-Enterprise Cooperation Projects (51900265005), portable, in car, on-line monitoring instrument development and demonstration for focusing on prevention and control of heavy metals like mercury, chromium, lead, cadmium, arsenic (2012YQ060115), the Fundamental Research Funds for the Central Universities (2652013101, 2652013086, 2652013087), and the Key Project of Air Pollution Causes and Control Technology Research (2016YFC0209205).

DATA AVAILABILITY STATEMENT

All relevant data are included in the paper or its Supplementary Information.

REFERENCES

Bai, S. & Shen, X. P. 2012 Graphene-inorganic nanocomposites. *Rsc Advances* **2** (1), 64–98.

Balko, B. A. & Tratnyek, P. G. 1998 Photoeffects on the reduction of carbon tetrachloride by zero-valent iron. *Journal of Physical Chemistry B* **102** (8), 1459–1465.

Boronina, T. & Klabunde, K. I. 1995 Destruction of organohalides in water using metal particles: carbon tetrachloride/water reactions with magnesium, tin, and zinc. *Environmental Science & Technology* **29** (6), 1511–1517.

Chen, X., Lv, X. F., Yang, Q., Wang, Y. Y., Jin, X., Wang, J. & Yang, Z. L. 2019 Dechlorination of carbon tetrachloride by nanoscale nickeled zero-valent iron @ multi-walled carbon nanotubes: impact of reaction conditions, kinetics and mechanism. *Applied Organometallic Chemistry* **33** (3), e4772.

Cwiertny, D. M., Bransfield, S. J., Livi, K. J. T., Fairbrother, D. H. & Roberts, A. L. 2006 Exploring the influence of granular iron additives on 1,1,1-trichloroethane reduction. *Environmental Science & Technology* **40** (21), 6837–6843.

Dahm, C. N. 1994 Chemical kinetics and process dynamics in aquatic systems by Patrick L. Brezonik. *Journal of the North American Benthological Society* **14** (2), 354.

Doherty, R. E. 2000 A history of the production and use of carbon tetrachloride, tetrachloroethylene, trichloroethylene and 1,1,1-trichloroethane in the United States: part 1—historical background; carbon tetrachloride and tetrachloroethylene. *Environmental Forensics* **1** (2), 69–81.

Dreyer, D. R., Park, S., Bielawski, C. W. & Ruoff, R. S. 2009 The chemistry of graphene oxide. *Chemical Society Reviews* **39** (1), 228–240.

Echigo, T., Hatta, T., Nemoto, S. & Takizawa, S. 2012 X-ray photoelectron spectroscopic study on the goethites with variations in crystallinity and morphology: their effects on surface hydroxyl concentration. *Physics and Chemistry of Minerals* **39** (9), 769–778.

Ertl, G., Kniizinger, H., Weitkamp, J., Professor, S. & Suslick, K. S. 1997 Handbook of heterogeneous catalysis, Vol. III. *Zeitschrift Für Physikalische Chemie* **208** (Part_1_2), 274–278.

Fan, Z. J., Kai, W., Yan, J., Wei, T., Zhi, L. J., Feng, J., Ren, Y. M., Song, L. P. & Wei, F. 2011 Facile synthesis of graphene nanosheets via Fe reduction of exfoliated graphite oxide. *ACS Nano* **5** (1), 191–198.

Feng, J. & Lim, T. T. 2005 Pathways and kinetics of carbon tetrachloride and chloroform reductions by nano-scale Fe and Fe/Ni particles: comparison with commercial micro-scale Fe and Zn. *Chemosphere* **59** (9), 1267–1277.

Fiedor, J. N., Bostick, W. D., Jarabek, R. J. & Farrell, J. 1998 Understanding the mechanism of uranium removal from groundwater by zero-valent iron using X-ray photoelectron spectroscopy. *Environmental Science & Technology* **32** (10), 1466–1473.

Gillham, R. W. & Ohannesin, S. F. 1994 Enhanced degradation of halogenated aliphatics by zero-valent iron. *Ground Water* **32** (6), 958–967.

Hashsham, S. A., Scholze, R. & Feedman, D. L. 1995 Cobalamin-enhanced anaerobic biotransformation of carbon tetrachloride. *Environmental Science & Technology* **29** (11), 2856–2863.

Hayes, M. 2001 Review of: Rase, H. F. Commercial heterogeneous catalysis. Handbook of commercial catalysts – heterogeneous catalysts. *Platinum Metals Review* **45** (2), 83.

Hua, I. & Hoffmann, M. R. 1996 Kinetics and mechanism of the sonolytic degradation of CCl4: intermediates and byproducts. *Environmental Science & Technology* **30** (3), 864–871.

Jin, X., Li, Q. & Yang, Q. 2018 The reactivity of Fe/Ni colloid stabilized by carboxymethylcellulose (CMC-Fe/Ni) toward chloroform. *Environmental Science & Pollution Research* **25** (21), 21049–21057.

Kustov, L. M., Al-Abed, S. R., Virkutyte, J., Kirichenko, O. A., Shuvalova, E. V., Kapustin, G. I., Mishin, I. V., Nissenbaum, V. D., Tkachenko, O. P. & Finashina, E. D. 2014 Novel Fe-Pd/SiO_2 catalytic materials for degradation of chlorinated organic compounds in water. *Pure and Applied Chemistry* **86** (7), 1141–1158.

Liu, R. & Lal, R. 2012 Nanoenhanced materials for reclamation of mine lands and other degraded soils: a review. *Journal of Nanotechnology* **2012**, 1–18.

Lowry, G. V. & Reinhard, M. 1999 Hydrodehalogenation of 1-to 3-carbon halogenated organic compounds in water using a palladium catalyst and hydrogen gas. *Environmental Science & Technology* **33** (11), 1905–1910.

Lv, X. F., Li, H., Ma, Y. Y., Yang, H. & Yang, Q. 2018 Degradation of carbon tetrachloride by nanoscale zero-valent iron @ magnetic Fe_3O_4: impact of reaction condition, kinetics, thermodynamics and mechanism. *Applied Organometallic Chemistry* **32** (3), e4139.

Matheson, L. J. & Tratnyek, P. G. 1994 Reductive dehalogenation of chlorinated methanes by iron metal. *Environmental Science & Technology* **28** (12), 2045–2053.

Moulder, J. F., Chastain, J. & King Jr, R. C. 1979 Handbook of X-ray photoelectron spectroscopy : a reference book of standard spectra for identification and interpretation of XPS data. *Chemical Physics Letters* **220** (1), 7–10.

Pei, S. & Cheng, H. M. 2012 The reduction of graphene oxide. *Carbon* **50** (9), 3210–3228.

Periasamy, M. & Thirumalaikumar, P. 2000 Methods of enhancement of reactivity and selectivity of sodium borohydride for applications in organic synthesis. *Journal of Organometallic Chemistry* **609** (1–2), 137–151.

Santharam, S., Davis, L. C. & Erickson, L. E. 2014 Biodegradation of carbon tetrachloride in simulated groundwater flow channels. *Environmental Progress & Sustainable Energy* **33** (2), 444–453.

Satterfield, C. N. 1991 *Heterogeneous Catalysis in Industrial Practice*, 2nd edn. McGraw-Hill Inc., New York, NY.

Schreier, C. G. & Reinhard, M. 1995 Catalytic hydrodehalogenation of chlorinated ethylenes using palladium and hydrogen for the treatment of contaminated water. *Chemosphere* **31** (6), 3475–3487.

Schrick, B., Blough, J. L., Jones, A. D. & Mallouk, T. E. 2002 Hydrodechlorination of trichloroethylene to hydrocarbons using bimetallic nickel-iron nanoparticles. *Chemistry of Materials* **14** (12), 5140–5147.

Semprini, L. & McCarty, P. L. 1992 Comparison between model simulations and field results for in situ biorestoration of chlorinated aliphatics. 2. Cometabolic transformations. *Ground Water* **30** (1), 37–44.

Smith, M. B. & March, J. 2001 *Advanced Organic Chemistry: Reaction, Mechanisms, and Structure*, 5th edn. Wiley, New York, NY, pp. 465.

Stankovich, S., Dikin, D. A., Piner, R. D., Kohlhaas, K. A., Kleinhammes, A., Jia, Y., Wu, Y., Nguyen, S. T. & Ruoff, R. S. 2007 Synthesis of graphene-based nanosheets via chemical reduction of exfoliated graphite oxide. *Carbon* **45** (7), 1558–1565.

Wang, X., Chen, C., Chang, Y. & Liu, H. 2009 Dechlorination of chlorinated methanes by Pd/Fe bimetallic nanoparticles. *Journal of Hazardous Materials* **161** (2), 815–823.

Wu, Y. W., Yue, Q. Y., Ren, Z. F. & Gao, B. Y. 2018 Immobilization of nanoscale zero-valent iron particles (nZVI) with synthesized activated carbon for the adsorption and degradation of Chloramphenicol (CAP). *Journal of Molecular Liquids* **262**, 19–28.

Yamashita, T. & Hayes, P. 2008 Analysis of XPS spectra of Fe^{2+} and Fe^{3+} ions in oxide materials. *Applied Surface Science* **254** (8), 2441–2449.

Zhang, W. X. 2003 Nanoscale iron particles for environmental remediation: an overview. *Journal of Nanoparticle Research* **5** (3–4), 323–332.

Zhang, W. X., Wang, C. B. & Lien, H. L. 1998 Treatment of chlorinated organic contaminants with nanoscale bimetallic particles. *Catalysis Today* **40** (4), 387–395.

Zhang, Y., Chen, L. X., Lei, Y. Q. & Wang, Q. D. 2002 The reduction of cycling capacity degradation of Mg-Ni-based electrode alloys by Fe substitution. *International Journal of Hydrogen Energy* **27** (5), 501–506.

Zhang, Q., Li, J., Miao, H. & Fu, J. 2011 Preparation of γ-Fe_2O_3/Ni_2O_3/$FeCl_3$($FeCl_2$) composite nanoparticles by hydrothermal process useful for ferrofluids. *Smart Materials Research* **2011**, 1–5.

Zhang, N., Zhang, Y. H. & Xu, Y. J. 2012 Recent progress on graphene-based photocatalysts: current status and future perspectives. *Nanoscale* **4** (19), 5792–5813.

First received 8 May 2020; accepted in revised form 2 August 2020. Available online 13 August 2020